CHALMERS
UNIVERSITY OF TECHNOLOGY

Advancing sustainable food processing: molecular-scale understanding of incipient protein fouling in falling-film evaporators

Journal of Food Engineering 406 (2026) 112816

Contents lists available at ScienceDirect

Journal of Food Engineering

journal homepage: www.elsevier.com/locate/jfoodeng

Advancing sustainable food processing: molecular-scale understanding of incipient protein fouling in falling-film evaporators

Mütesir Temel [a], Sadiye Velioğlu [b], Anders Hellman [c], Jia Wei Chew [a,*]

[a] Department of Chemistry and Chemical Engineering, Chalmers University of Technology, 412 96, Gothenburg, Sweden
[b] Institute of Nanotechnology, Gebze Technical University, 41400, Kocaeli, Türkiye
[c] Department of Physics and Competence Centre for Catalysis, Chalmers University of Technology, Göteborg, Sweden

ARTICLE INFO

Keywords:
protein fouling
Food processing
Molecular dynamics simulation
Adsorption behavior
Coulombic interactions
Food sustainability

ABSTRACT

Aligned with the green transition of the food industry, this study addresses the downstream processing of food protein ingredients from novel sources and enhanced production methods. As with current liquid foods (e.g., milk), reducing the water content to create concentrates or powders is necessary for longer shelf-life and ease of transport. A dominant unit operation for this purpose is the falling-film evaporator (FFE). This study focuses on the inevitable protein-fouling issue of FFEs that limits energy efficiency. To understand the incipient adsorption behavior (i.e., fouling behavior at the initial stages) of a model protein (namely, lysozyme) onto the chromium (III) oxide (Cr_2O_3) surface of the stainless-steel heat-transfer surface of FFEs, molecular dynamics simulations were performed. Six lysozyme orientations were initialized at four temperatures each. Results indicate adsorption is primarily governed by attractive electrostatic interactions by basic amino acid residues, whereas acidic amino acids tend to be repulsive due to the negative charges. Temperature effects are secondary to local interactions, with no clear correlation with adsorption tendencies, suggesting the onset of fouling is temperature independent. The adsorption tendencies of amino acid residues onto Cr_2O_3 revealed here are expected to be valuable for providing insights into FFE-fouling by emerging food protein formulations.

1. Introduction

To ensure food sustainability, the transition from traditional meat-based to alternative food sources is accelerating (Fasolin et al., 2019), (Loveday, 2019). Much attention has been directed to identifying novel sources, but the inevitable downstream processing to produce high-quality protein ingredients is lagging. Generally, food ingredients require long shelf-life, typically achieved by turning the liquid food (i.e., water-based food suspensions or emulsions) into dried powder with sufficiently low water activity. For milk, the conventional practice is to employ a series of falling-film evaporators (FFE) followed by spray-drying (Ledenbach and Marshall, 2009) to obtain milk powder for ambient storage (Lewis and Lewis, 2023). Energy-efficient alternatives like membrane filtration are gaining attention, but challenges like limited concentration of solids, membrane-fouling, and high membrane replacement costs restrict their application (Gulied et al., 2023), (Cassano et al., 2020) (Wilson, 2018). Freeze concentration presents an alternative option, but the solids concentration is limited due to the corresponding increase in viscosity (Miyawaki and Inakuma, 2021). Among multi-effect evaporators, FFEs are the most common due to the ease of operation (Cyklis, 2022), though they persistently suffer from inefficiencies like fouling of the heat-transfer surfaces, causing materials loss, downtime and high energy use (Jebson and Iyer, 1991) (Díaz-Ovalle et al., 2017) (De Jong, 1997). Furthermore, spray-drying still struggles with high-viscosity long-chain proteins, complicating atomization (Dantas et al., 2024). Compared to spray-drying dilute feedstocks, FFE ensures both gentle product processing as well as relatively reduced energy consumption (Sim et al., 2023). These challenges may worsen with new protein formulations. For efficient processing of emerging proteins, this study focuses on bridging the knowledge gaps on how to adapt the FFE, which is a dominant unit operation in the food industry and is responsible for 76 % of exergy destruction rate in milk powder production (Yildirim and Genc, 2017).

The falling-film evaporator (FFE) represents one of the most prevalent evaporative water removal units in not only the food industry, but also in other industries like forestry, chemicals, etc. It operates such that the liquid food enters at the top, is distributed as thin liquid films on the inside of the steam-heated tubes and flows downwards by gravity. In the

* Corresponding author.
E-mail address: jia.chew@chalmers.se (J.W. Chew).

https://doi.org/10.1016/j.jfoodeng.2025.112816
Received 26 March 2025; Received in revised form 19 August 2025; Accepted 8 September 2025
Available online 13 September 2025

food industry, to ensure high thermal efficiency while mitigating heat damage, the upper limits of operating temperatures are 50 °C for fruit juices (Cyklis, 2022) and 70 °C for milk (Morison, 2015a). While such food processing methods are critical to prolong shelf-life, the efficiency of the FFE remains poor due to multiple challenges like fouling (Cyklis, 2022), (Liu and Delaplace, 2024a,b), (Tuoc, 2015), resulting in 50 % of the energy in milk powder manufacturing being exhausted by the FFE (Jebson and Iyer, 1991). A key challenge of FFEs is the fouling of the heat-transfer surfaces by proteins, which accounts for 40 % of production costs due to the loss of milk solids as fouling deposits, and cleaning costs involving downtime, chemicals, water, and waste disposal (Morison, 2015b). In particular, FFEs are particularly susceptible to fouling caused by the concentration of proteins at the heat-transfer surface during thermal processing. Protein fouling is a multi-stage phenomenon involving transport to the surface, initial adsorption, conformational rearrangement, aggregation, and consolidation into a fouling layer (Rabe et al., 2011). Earlier studies have explained how different fouling mechanisms are affected by the processing conditions (e.g., pH, milk age) involved in the heat treatment of milk (De Jong, 1997). The influence of protein charge, thermal stability, and hydrophobicity in promoting or reducing fouling has been further reported, as well as the effect of vacuum evaporation within FFEs inducing several physicochemical and rheological changes that contribute to fouling (Tuoc, 2015), (Liu and Delaplace, 2024a,b. These changes not only affect heat-transfer performance but also influence product quality by promoting protein denaturation, aggregation, and potential loss of nutritional value (De Jong, 1997). Therefore, understanding and controlling fouling is essential not only for maintaining process efficiency, but also for functional (e.g., emulsification) and nutritional properties in protein-rich foods (A. L. and S. P. and J. R. et al., 2016). Because proteins are essential components in a wide range of food products to impart distinct functional and nutritional attributes, the mechanisms underlying protein fouling during food processing warrants in-depth understanding.

Molecular dynamics (MD) simulations have provided molecular-level understanding of the incipient fouling phenomena in other applications (e.g., membrane fouling (Ma and Chew, 2022a)). A challenge with macromolecular foulants like proteins is that macroscopic characterizations, like overall electrical charge, are acknowledged to be poorly correlated with membrane fouling (Ma et al., 2021a), (Ma et al., 2021b). Experimental methods largely fall short of providing such protein-scale resolution. The employment of MD simulation in the food field is quite nascent, with applications expanding from small molecules to macromolecules and even complex systems containing various interacting molecular groups (Singh et al., 2018). The focus here is on employing MD simulations to understand protein adsorption (i.e., fouling) onto the heat-transfer surface of an FFE.

Previous studies have shed some light on the adsorption mechanisms of proteins on various surfaces. Due to the macromolecular structure and heterogeneous local charges, experimental results are somewhat limited, and MD simulations have been very valuable in providing detailed molecular-level insights. Protein properties such as surface charge, hydrophilicity, and electronic properties have been reported to impact protein-surface interactions (Zhou and Pang, 2018) (Panczyk et al., 2022). Also, the impact of different adsorbent surfaces, such as metals (including gold, iron, and silver), metal oxides (like TiO_2 and MgO), clays, and carbon-based materials (such as graphene oxide) have been studied, with the overall conclusion that protein-surface interactions are largely driven by charges (Antosiewicz and Długosz, 2020) (Sahihi and Faraudo, 2022) (Wei et al., 2012). Zhang et al. (2022a) revealed that negatively charged oxygen atoms on bovine serum albumin (BSA) and magnesium ions (Mg^{2+}) on the magnesium alloy surface underlie the strong interactions. In addition, Utesch et al. (2013) studied how nickel-iron (NiFe) hydrogenase interacted with modified gold surfaces, with results indicating that residues possessing reactive groups such as hydroxide (OH) and carboxylic (COOH) groups play important roles in the interactions. Building on the knowledge base, the focus here is on how proteins interact with the protective chromium (III) oxide (Cr_2O_3) coat of the stainless-steel heat-transfer tubes in FFEs.

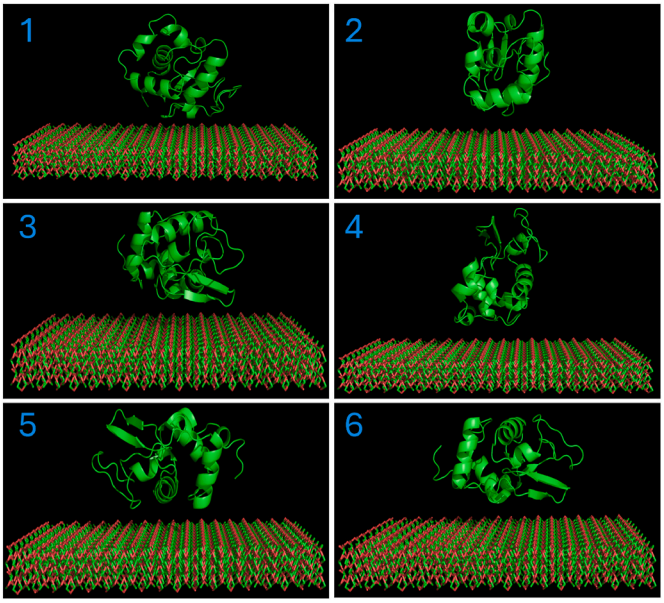

Fig. 1. 3D simulation domains depicting the fixed Cr_2O_3 slabs and lysozymes initialized at six different orientations.

In this study, the overarching objective is to understand the adsorption (i.e., fouling) behaviors of lysozyme onto the stainless-steel surface of the FFE (i.e., the chromium (III) oxide (Cr_2O_3) layer than confers corrosion resistance to all grades of stainless steels) over the operational range of temperatures. Noting that bovine milk alone contains hundreds of types of proteins (Tuoc, 2015), the goal here is instead to understand the preferential adsorption tendencies of the protein primary structure (i.e., the amino acid constituents) through a model, well-studied protein molecule, and thereby extend the knowledge gained to other proteins. Six lysozyme orientations were initialized at four temperatures each (namely, 293 K, 303 K, 313 K, and 333 K). While the lower limit is for experimental validation, the upper limit is to mimic industrial FFE operating temperatures (Cyklis, 2022), (Morison, 2015a) as well as to avoid denaturation effects. The total interaction and binding energies were quantified, along with the demarcation into Coulombic and Lennard-Jones contributions. Then, the minimum lysozyme-Cr_2O_3 distances were quantified. Also, the local adsorption sites were identified, and the preferential affinities of the four categories of amino acid residues (namely, acidic, basic, neutral nonpolar, and neutral polar) were revealed. Additional characterizations were presented, including root-mean-square deviation (rmsd), root-mean-square fluctuation (rmsf), radius of gyration (Rg), number of lysozyme-Cr_2O_3 contacts, and number of intra-lysozyme hydrogen bonds. It should be noted that, while MD simulations are useful in revealing molecular-scale dynamics at incipient fouling, the spatiotemporal limitations restrict direct links to macroscopic phenomena like heat transfer and foulant buildup.

2. MATERIAL and METHOD

2.1. Adsorbate and adsorbent

The lysozyme molecule, which consists of 129 amino acids (PDB ID:8F28), was downloaded from the RCSB Protein Data Bank, and then uploaded onto CHARMM-GUI to remove water and all other molecules (e.g., ligand, substrate). Since local interactions have been reported to affect protein adsorption tendencies (Antosiewicz and Długosz, 2020)

(Zhang et al., 2022a), the lysozyme molecule was initialized at six different orientations by rotating at various multiples of 90° around the *x* and *y* axes.

To represent the surface of the stainless-steel surface of the falling-film evaporator (FFE), chromium (III) oxide (Cr_2O_3), which is the protective coating that prevents corrosion (Zhang et al., 2022b), was generated. Specifically, a rectangular Cr_2O_3 slab (Fig. 1) with dimensions of 77.3 Å by 81.6 Å, and thickness of 9.9 Å, was created by using CHARMM-GUI's Nanomaterial module.

2.2. Simulation setup and procedure

The 3D simulation domain (with dimensions of 9 nm by 9 nm by 9 nm) that contained all the components (namely, lysozyme, Cr_2O_3 slab, solvent molecules, and ions) was generated using the MultiComponent assembler module in CHARMM-GUI.

The Cr_2O_3 slab was fixed at the bottom of the simulation box. At the beginning of the simulation, lysozyme was centered above the Cr_2O_3 slab and the minimum distance between the lysozyme and the Cr_2O_3 surface was set at 5 Å, as depicted in Fig. 1. Ionic strength (namely, Na^+ and Cl^- ions) mimicking 15 mM of NaCl was adjusted to neutralize the system. For simulating water as solvent molecules, TIP3P (Toukan and Rahman, 1985) CHARMM36FF parameters were adopted. Periodic boundary conditions (PBC) were applied.

GROMACS 2024v2 was utilized with CHARMM36 force field to prepare all systems, perform the all-atom MD simulations, and analyze trajectories. It should be noted that only CHARMM27 is available in GROMACS, so the required files for CHARMM36 with cmap correction were obtained from MacKerell Lab website (Best et al., 2012) and integrated accordingly. Moreover, Cr_2O_3 does not have the CHARMM force field parameters. To address this, in the CHARMM-GUI, the values for the atoms originally adapted from the Interface force field were appropriately converted into CHARMM36 parameters (Kanhaiya et al., 2021) (Zhuang et al., 2020).

After preparation of the simulation domain, energy minimization was the first step performed to a maximum of 100 $kJmol^{-1}nm^{-1}$ force using the Verlet cut-off scheme with H-bonds constraints and the LINCS algorithm. The cut-off for long-range electrostatic and van der Waals interactions was set to 12 Å with the Particle Mesh Ewald summation (PME) (Darden et al., 1993). The update frequency for the neighbor list was scaled to 1 ps^{-1}. By using the steepest descent algorithm, conversion of each orientation of lysozyme to its local minimum within 50,000 cycles was carried out, after which equilibration steps ensued.

For all the equilibration and production steps, the time step was adjusted to 1 fs. The equilibration for all orientations was performed within three steps using Langevin dynamics. For the first equilibration step, an NVT ensemble was used and run for 1 ns. Then, two more equilibration steps followed using the NPT ensemble. The orientations were equilibrated (Berendsen) to 1 atm pressure for 250 ps, followed by isotropic pressure coupling (Parrinello-Rahman) for 1 ns to the same reference pressure. After that, four temperatures, namely, 293 K, 303 K, 313 K, and 333 K, were evaluated for each of the six lysozyme orientations (Fig. 1). During the all-equilibration steps, position restraint was applied to all heavy atoms (i.e., all atoms in the medium such as carbon and oxygen, except hydrogen) for both lysozyme and Cr_2O_3, which was adjusted with a force constant (k_{pr}) of 1000 $kJmol^{-1}nm^{-2}$. Once equilibrated, a 100 ns MD simulation was run, and trajectories at 10,000-step intervals were saved for a total of 10,000 frames per trajectory. Notably, in such limited time scale for each MD run, the foulant may not have sufficient time to orientate itself favorably to adsorb, and thus a common circumvention means is to run replicates starting from different initial foulant orientations to enhance statistical validity (Cummings et al., 2021), (Ma and Chew, 2022b), as was done here. Specifically, the different initial orientations facilitate interactions between different domains of the macromolecular lysozyme and the Cr_2O_3 slab.

Numerous parameters that reflect adsorption tendency were assessed at 10 ps intervals throughout each simulation run, including radius of gyration, hydrogen bonding (including intra-lysozyme and lysozyme-Cr_2O_3), root-mean-square deviation (rmsd), root-mean-square fluctuation (rmsf), number of contacts, binding free energy, interaction energy, and minimum distance between lysozyme or specific amino acid to Cr_2O_3. Details on the formulas used are presented in Section S1 in the Supporting Information. Where necessary to reduce noise, exponential smooth approximation was utilized.

2.3. Quartz crystal microbalance with dissipation (QCM-D)

QCM-D, which is a highly sensitive analytical technique used to measure mass changes due to adsorption onto surfaces in real time, was used to provide experimental data for model validation. Lysozyme was purchased from Sigma-Aldrich (Product Number: 62971). The phosphate buffer solution (PBS) was prepared by mixing 8 g of NaCl (VRW Chemicals, CAS Number: 7647-14-5), 1.44 g of Na_2HPO_4 (Merck, CAS Number: 10028-24-7), 0.2 g of KCl (SigmaAldrich, Product Number: P5405) and 0.24 g of KH_2PO_4 (Sigma-Aldrich, Product Number: P5655) with 800 mL of Milli-Q water. The solution was stirred using a magnetic stirrer for 1 h at ambient temperature. To set the pH of this stock solution to 7, HCl (1 M, Fisher, Product Number: 15675270) was used and distilled water was added until the total volume reached 1 L. The concentration of lysozyme was adjusted to 5 mg/mL and mixed with PBS for a final volume of 50 mL. Furthermore, 1 wt% SDS (Fisher, Product Number: BP166) and 3 wt% NaOH (Sigma—Aldrich, CAS Number: 131073-2) solutions were prepared with distilled water for cleaning.

QCM-D measurements were carried out with a Q-Sense E4 system and Ismatek high-precision multichannel dispenser. Voight modeling and curve fitting was performed with the instrument specific software package Qtools using overtone 3. A fresh stainless-steel sensor (Biolin Scientific, Product Number: SS2343), which mimicks the surface of the FFE evaporator, was positioned in the flow cell for each test. The flow cell was maintained at 293, 303, or 313 K. First, Milli-Q water was flowed through the cell for 10 min and the resonant frequency (f) was zeroed, after which PBS was flowed through for another 10 min. Then, 5 mg/mL of lysozyme in PBS was introduced to the flow cell at a constant flow rate of 0.15 mL/min over 40 min, during which changes in resonant frequency (Δf) were monitored. Notably, a decrease in Δf indicates an increase in the mass adsorbed onto the stainless-steel sensor surface. For each temperature, the test was repeated 3 times.

After each test, cleaning of the flow cell ensued by flowing PBS for 10 min, then 1 wt% NaOH for 10 min, and then 1 wt% SDS at 313 K for 10 min. After that, the sensor was removed, and rinsed with ethanol before drying with a nitrogen spray gun, and finally re-installed into the QCM-D.

3. Results and discussion

The results of six initial lysozyme orientations at four temperatures each (namely, 293 K, 303 K, 313 K, and 333 K) were obtained in this study. Based on an earlier study that indicated local interactions dominate (Díaz-Ovalle et al., 2017), instead of repeating runs at the same initial orientation, initialization at six different orientations was performed (Fig. 1). Nonetheless, to ascertain repeatability for the same initial orientation, two production runs were conducted at the same initial orientation, namely, Orientation 4, at 293 K (Fig. S1). Thus, for results pertaining to Orientation 4 at 293 K, averages are presented. The parameters that reflect adsorption and thereby fouling behaviors are presented as follows.

3.1. Model validation

As model validation, the protonation state (or total charge) of lysozyme was determined at pH = 7.0 with CHARMM-GUI (Brooks et al., 1983), as well as with GROMACS for cross-checking, to be +8e, which

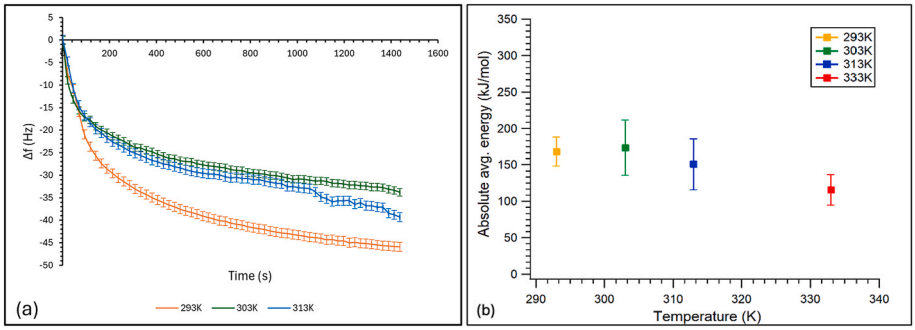

Fig. 2. (a) QCM-D results: Rate of mass of lysozyme collected onto the stainless-steel sensor surface at different temperatures. (b) Average interaction energies of all orientations with respect to temperature. The error bars represent standard errors.

agrees with an earlier study (Wei et al., 2012).

Additional validation via QCM-D experiments was performed at three temperatures, namely, 293 K, 303 K, and 313 K. Fig. 2a shows that the change in frequency (Δf in Hz) consistently becomes more negative with time, which reflects the progressive increase in lysozyme adsorbed onto the stainless-steel sensor. The steepest decline rate is for the system at 293 K, indicating the greatest affinity of lysozyme to the stainless-steel surface at this lowest temperature. However, the lowest decline rate was for the intermediate temperature of 303 K. This implies a non-monotonic relationship between temperature and adsorption tendency of lysozyme, which suggests that temperature is not a dominant influence on the affinity between lysozyme and stainless-steel.

To determine the total interaction energy to gauge the strength of adsorption of lysozyme onto stainless steel, the Coulombic and Lennard-Jones (LJ) energies were summed up and averaged over the last 50 ns of each 100 ns simulation. Fig. 2b summarizes the effect of temperature by averaging the interaction energies across all six orientations. To ascertain if the means are equal among the different temperatures, the ANOVA (Analysis of Variance) test for comparing multiple means was employed. At a 95 % confidence level, the null hypothesis is that all the means are equal, while the alternative hypothesis is at least one mean is different. The resulting p-value is 0.61, which is greater than 0.05 and thus fails to reject the null hypothesis. This implies that there is no significant difference among the means at the four temperatures, which is in sync with the QCM-D results on temperature not being a governing influence of lysozyme – stainless-steel interactions.

Although MD simulation numerically integrates Newton's equations of motion to predict the time evolution of a molecular system, the initial velocities of atoms are randomly assigned, and thus some variabilities between the results of repeated runs are inevitable. To assess the discrepancy between repeats, another production run for lysozyme initialized at Orientation 4 at 293 K was performed. Between the runs, some variabilities in the positions of the lysozyme molecules can be visually observed at 0 ns (i.e., start of the production run), 50 ns, and 100 ns in Fig. S1. Furthermore, Fig. S2 presents snapshots of the repeated runs at the three time points, along with the corresponding interaction energies. The interaction energies between the two runs are distinctly different. For example, at 100 ns, the interaction energy is −245 kJ/mol in one case and −84 kJ/mol in the other. In the former case, two hydrogen bonds formed between the NH_3^+ group of arginine and oxygen atom of Cr_2O_3 surface. In the latter, two basic amino acids (namely, arginine-125 and arginine-128) and a polar amino acid (namely, asparagine) are within 5 Å of Cr_2O_3. Moreover, Fig. S3a - e display the differences between the repeats with respect to the evolution of the parameters of rmsd, total interaction energy, Rg, minimum distance (between lysozyme and Cr_2O_3), and number of contacts, demonstrating the discrepancies between repeats. As for the residue distance with respect to residue number, Fig. S3f indicates similar trends between the repeats. In the following, for results pertaining to Orientation 4 at 293 K, averages are presented.

3.2. *Overall interaction energy*

The correlation between interfacial interaction energy and fouling

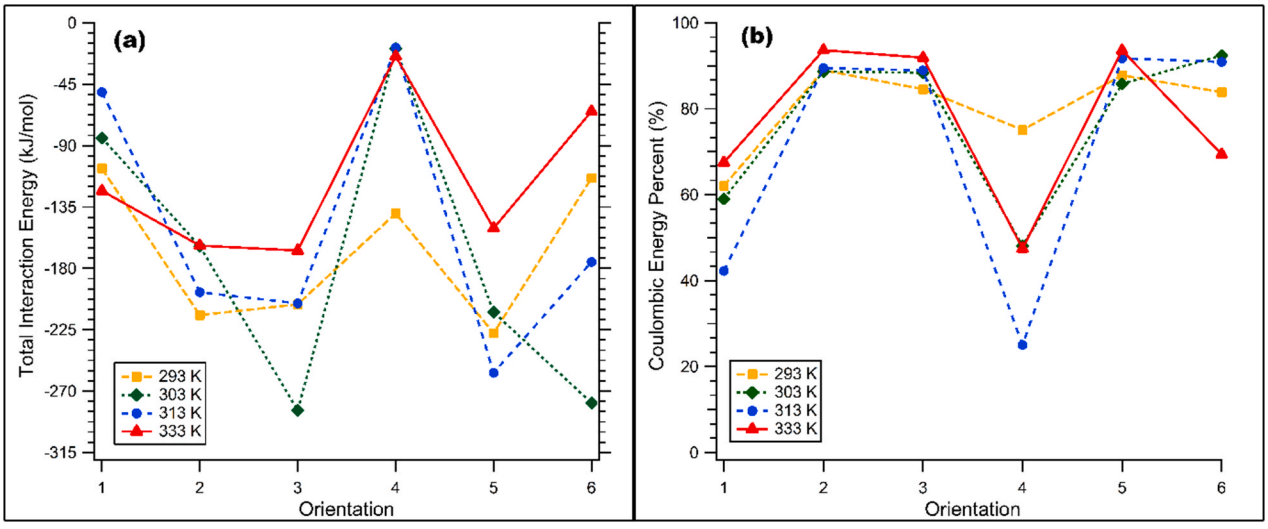

Fig. 3. Effect of initial lysozyme orientation and temperature on (a) total interaction energy (which is the sum of Coulombic and Lennard-Jones interactions), and (b) percentage of Coulombic interaction energy with respect to the total interaction energy.

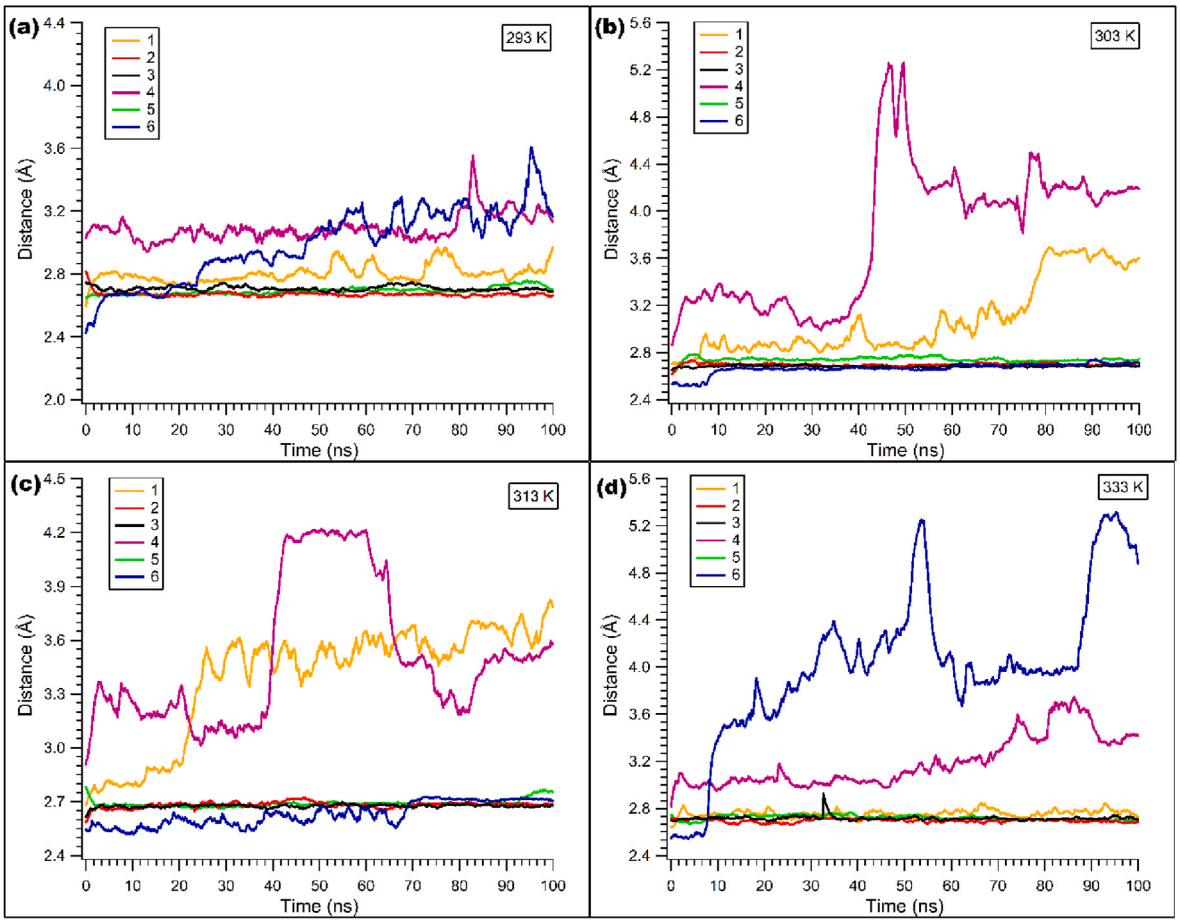

Fig. 4. Evolution of minimum distance between lysozyme and Cr_2O_3 (i.e., between the two closest atoms on each) with time at (a) 293 K, (b) 303 K, (c) 313 K, and (d) 333 K.

(e.g., membrane fouling (Chew et al., 2020), marine biofouling (Qiu et al., 2022)) is well acknowledged. Fig. 3a presents the average lysozyme-Cr_2O_3 interaction energies at four different temperatures and for six different initial lysozyme orientations in the final 50 ns of each 100 ns simulation. In addition, Fig. 4 displays the evolution of the lysozyme-Cr_2O_3 distance throughout the 100 ns of production run, which reflects whether lysozyme spontaneously adsorbs to the Cr_2O_3. Furthermore, as another way of representing the interactions, the binding energy was also computed, as shown in Table S1. Binding energies and interaction energies (Section S1) give similar trends. While potential of mean force (PMF) calculations via biased MD simulations can additionally provide the adsorption energy as a function of displacement, unbiased MD simulations were employed here to avoid the complication with regards to the impact of the additional external force imposed (Ma and Chew, 2022b).

The correlation between temperature and total interaction energy appears to be affected by the initial orientation. To determine if the interaction energy means are equal among the six orientations, the ANOVA (Analysis of Variance) test for comparing multiple means gives a p-value of 0.0019, which is less than 0.05 and thereby rejects the null hypothesis. This indicates that at least one of the mean interaction energies among the orientations is different at the 95 % confidence level. Therefore, whereas the effect of temperature on interaction energies is negligible, the effect of orientation is statistically non-negligible.

Four observations are worth noting. Firstly, among the temperatures, 333 K resulted in the least negative interaction energies for three out of the six orientations (namely, Orientations 3, 5, and 6). If temperature effects are significant, the initial orientations of lysozyme should have less effect on the adsorption tendency. This is not the case, which indicates that temperature is not a dominant influence on lysozyme-Cr_2O_3 affinity. Secondly, the influence of temperature is the least in the case of Orientation 2, while greatest in the case of Orientation 6. This suggests that temperature may affect different specific bindings (e.g., anchoring of specific amino acids) differently. Thirdly, the influence of orientation is the least at 293 K, while the greatest at 303 K. The significant variation in interaction energies across orientations at 303 K underscores that local interactions are strongly dependent on the spatial arrangement of amino acid residues relative to the Cr_2O_3 surface. These conformational effects are intrinsic to lysozyme and cannot be easily varied by temperature changes (Eleftheriou et al., 2006). Fourthly, among the orientations, the relationships between temperature and total interaction energy are not consistent. For instance, the most attractive energy for Orientation 3 is at 303 K, while that for Orientation 4 is at 293 K. Thus, as with the previous observations, this ascertains that an interplay between temperature and orientation effects dictates the strength of adsorption. Collectively, Fig. 3a highlights that the local interaction governed by the initial lysozyme orientation plays an important role in dictating the tendency of lysozyme to adsorb onto stainless steel. This agrees with earlier studies on the dominance of local interactions by the specific amino acid residues in affecting adsorption, rather than the macroscopic parameters (e.g., zeta potential, pH) (Wei et al., 2012) (Antosiewicz and Długosz, 2020) (Zhou and Pang, 2018).

Fig. 3b displays the percentage of the total interaction energy contributed by Coulombic interactions, with the rest being by Lennard-Jones (LJ). Clearly, Coulombic interactions are relatively more dominant in governing the adsorption behavior, with the values generally more than 50 % and up to 93 %. This implies that charge-based interactions, specifically the different charges on the amino acid residues

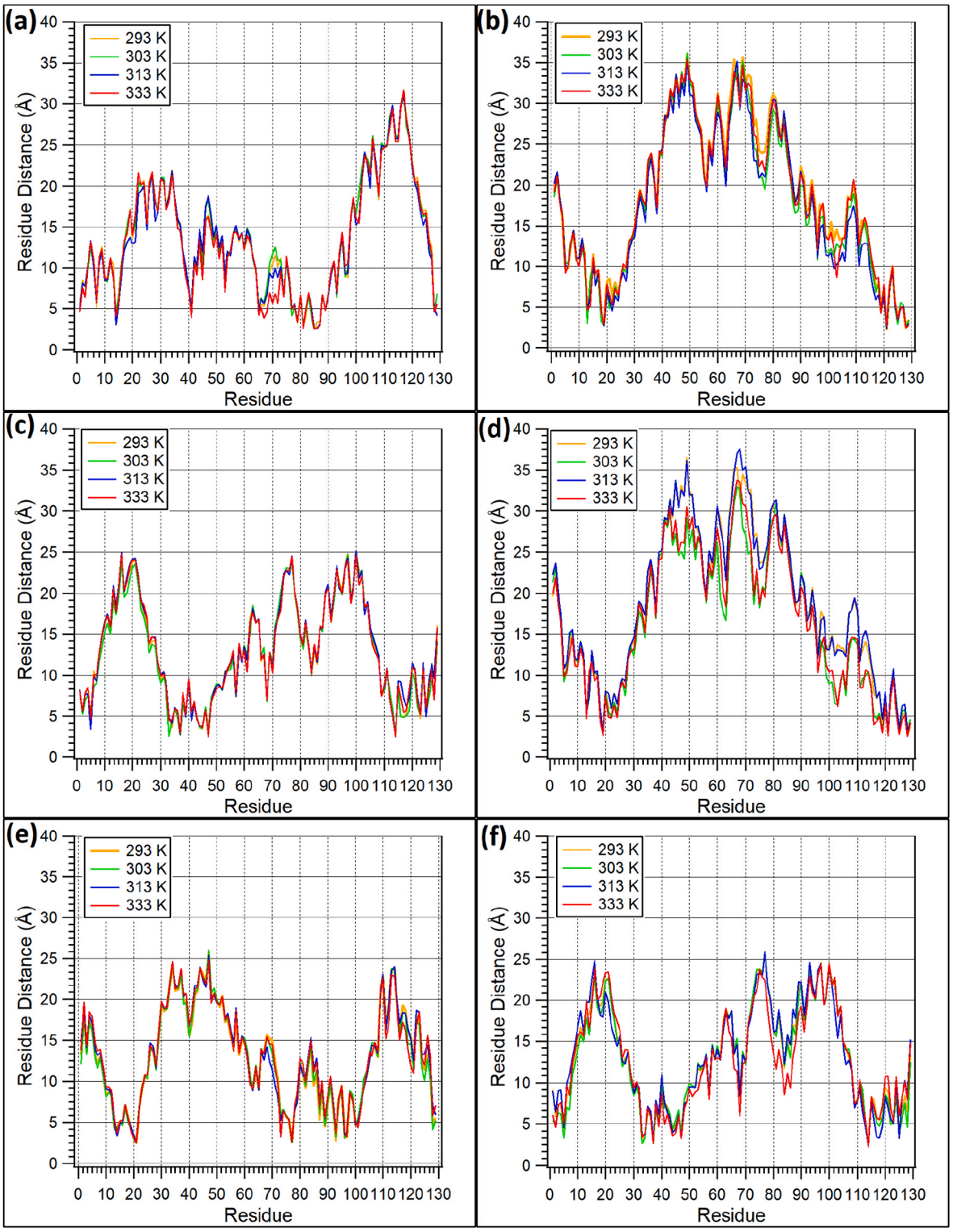

Fig. 5. The average distance of each amino acid residue of lysozyme to the Cr_2O_3 slab for different initial orientations. **a-f** represent orientations 1–6.

(e.g., negatively charged acidic residues versus positively charged basic residues), are more influential in governing the physical interactions.

It is worth noting that the negligible impact of temperature for lysozyme adsorption onto Cr_2O_3 revealed here governs only the incipient fouling step. The mechanisms underlying the correlation or lack thereof between temperature and subsequent fouling stages involving aggregation and conformational changes (e.g., denaturation) (Tuoc, 2015) warrant further investigations.

3.3. Minimum distance

As the simulation progresses, while the position of the Cr_2O_3 slab is fixed, the lysozyme molecule is free to move towards or away from it depending on the affinity between the residues on lysozyme and Cr_2O_3. Thus, quantifying the minimum distance between lysozyme and Cr_2O_3 (i.e., between the two closest atoms on each) provides indications of the affinity between the two entities. Fig. 4 presents the minimum distance

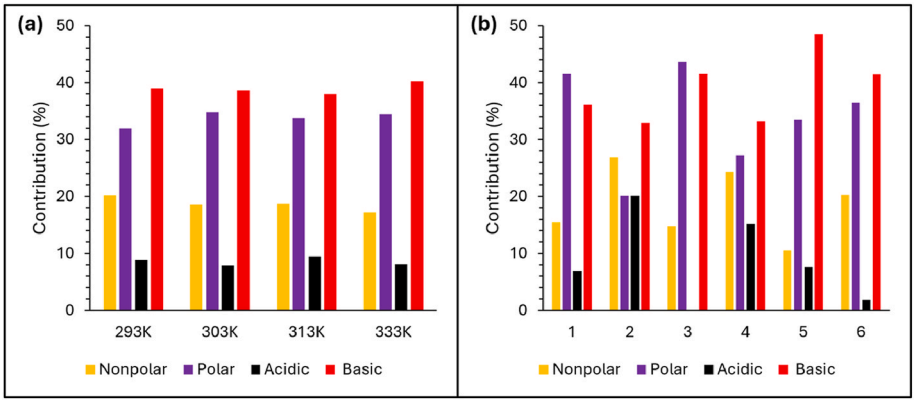

Fig. 6. Number-based contribution of each category of amino acid (namely, neutral nonpolar, neutral polar, acidic, and basic) to lysozyme adsorption based on the amino acid being 5 Å or less from the Cr_2O_3 slab.

between the lysozyme and Cr_2O_3 surface. In some cases, the trends are flat with minimum distance values of 3 Å or below, which indicates that the lysozyme molecule is adsorbed firmly to the Cr_2O_3 surface. In other cases, the minimum distances computed fluctuate at higher values, indicating that the lysozyme does not adsorb. As expected, the systems having low total interaction energies (Fig. 3a) and binding energies (Table S1) exhibit higher minimum distances. For example, for the least attractive interaction energies shown in Fig. 3a for the cases of Orientation 4 at temperatures of 303–333 K, the corresponding minimum distances are clearly higher in Fig. 4. Furthermore, Fig. 4 reflects that five of the six cases have adsorbed at 293 K, while four of the six cases have adsorbed at 303, 313, and 333 K. Of the non-adsorbed cases, only initial orientations of 1, 4, and 6 are involved. Comparing these cases with Fig. 3a indicates that total interaction energies of above 100 kJ/mol in magnitude are needed to warrant the adsorption of lysozyme onto Cr_2O_3.

3.4. Adsorption sites

While it is exceptionally challenging experimentally to identify which amino acid is interacting with the Cr_2O_3 slab, MD simulations can readily achieve this. Fig. 5 presents the distance between each amino acid residue and the Cr_2O_3 slab, reflecting how the chain of 129 amino acid residues that make up lysozyme aligns with respect to the Cr_2O_3 slab. Furthermore, Fig. S4–S9 quantify the residue-Cr_2O_3 distances of four residues that get to within 5 Å of the Cr_2O_3 slab (namely, basic Lys, basic Arg, polar acidic Glu, and polar acidic Asp) resulting from the six different initial orientations. Two observations are notable. Firstly, for the different orientations, it appears that it is not always the same amino acid residues that anchor onto Cr_2O_3. For instance, comparing Orientations 1 (Figs. 5a) and 2 (Fig. 5b) indicates the first residue (i.e., Lys-1) is close to Cr_2O_3 in the former case (5 Å or less; Fig. S4) but much further away for the latter (almost 20 Å; Fig. S5). Secondly, the different temperatures assessed have limited influence on the residue distance trends, indicating that the preferential affinity of specific amino acid residues to Cr_2O_3 exceeds the temperature effects. For instance, in the case of Orientation 6, temperature has the most significant influence on total interaction energy (Fig. 3a), and Fig. 5f shows clearly the preferential binding and non-binding by specific amino acid residues. As Fig. S9 indicates, regardless of temperature, residue 114 (i.e., Arg-114) remains tightly bound (<5 Å) to Cr_2O_3, while residue 1 (i.e., Lys-1) fluctuates within a narrow distance range of 5–10 Å across the temperatures. Therefore, Fig. 5 emphasizes the importance of the local amino acid residue interactions in influencing adsorption.

3.5. Preferential affinity of amino acid residues

Recalling that the lysozyme was initialized at a minimum distance of 5 Å from Cr_2O_3, a residue distance of less than 5 Å implies attraction. Since Fig. 3b indicates charged interactions govern the adsorption

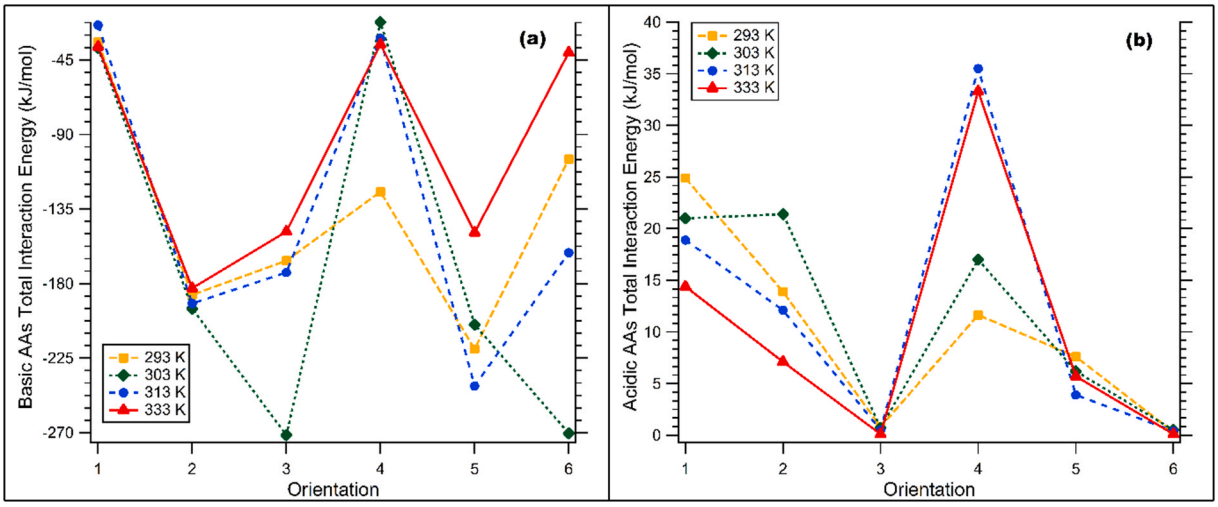

Fig. 7. The total interaction energies in the last 50 ns of each 100 ns simulation: (a) basic amino acids (namely, lysine, arginine, and histidine), and (b) acidic amino acids (namely, acetic acid and glutamic acid).

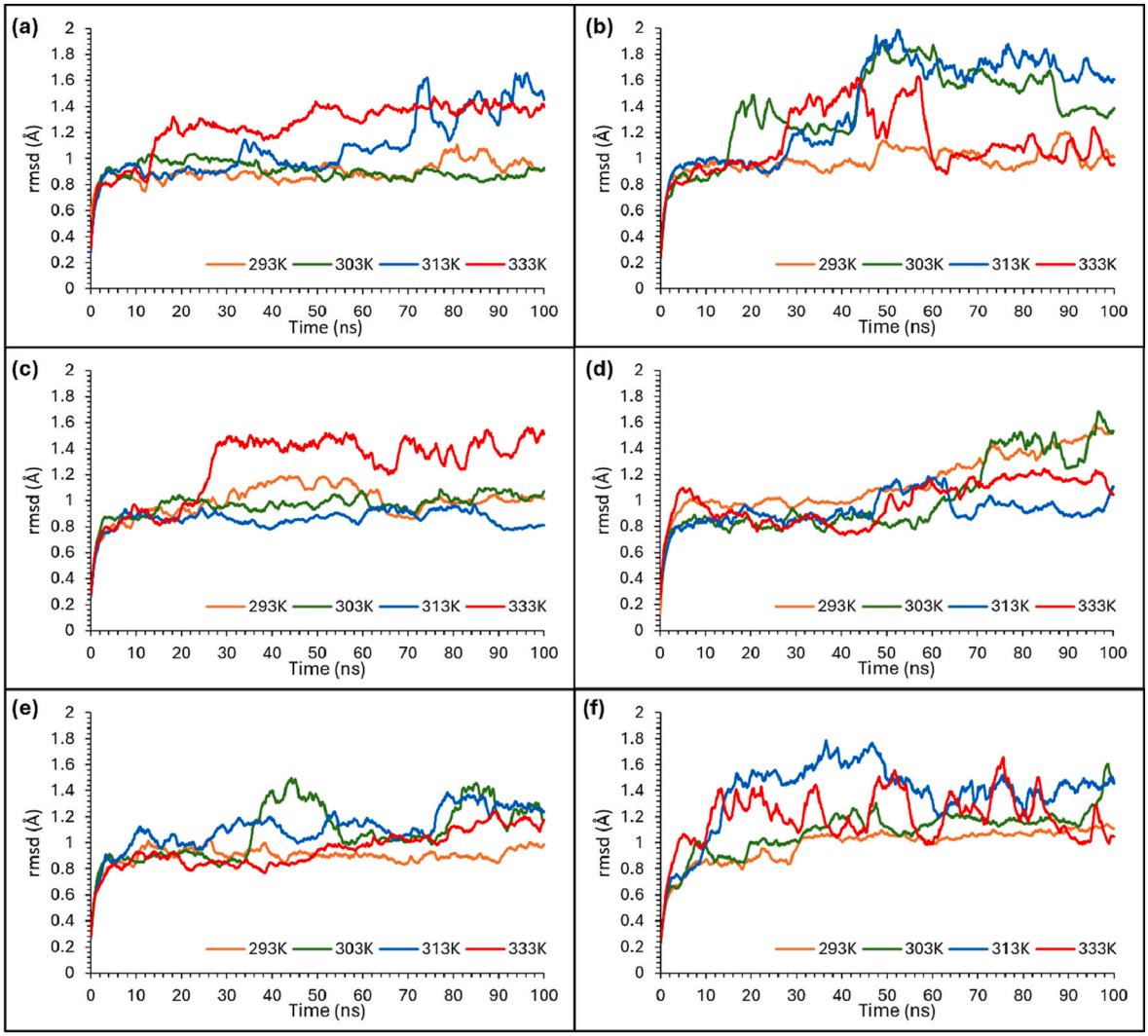

Fig. 8. Changes in rmsd values of lysozyme-Cr_2O_3 systems over time for six initial orientations at four different temperatures. **a-f** represent Orientations 1–6.

behavior, a closer inspection of the different categories of amino acids (namely, neutral nonpolar, neutral polar, acidic, and basic) was taken. Specifically, all the amino acids that are 5 Å or less from the Cr_2O_3 slab were identified, then classified into the four categories, and finally, the number-based percentage of each category was computed. Fig. 6a shows that, at all temperatures, the basic amino acid residues are the most dominant in influencing lysozyme adsorption (37–40 %), followed by neutral polar (30–34 %) and neutral nonpolar (17–21 %), while the acidic ones are the least influential (7–10 %). With regards to initial orientation, Fig. 6b shows that acidic residues remain least probable to be close to Cr_2O_3, while the basic and neutral polar ones are more likely.

The prominence of basic and neutral polar amino acid residues in close proximity with Cr_2O_3 (<5 Å) shown in Fig. 6 and the dominance of Coulombic interactions shown in Fig. 3b are in agreement. Cr_2O_3 is amphoteric and typically exhibits a partially negatively charged surface in aqueous environments, with mostly oxygen atoms exposed. It should be noted that the pK_a values for the basic amino acid residues are between 9 and 14, while that for the acidic ones are between 1 and 5. Thus, at pH = 7, almost all basic residues except histidine are in the protonated state, which means they tend to be positively charged due to the excess number of hydrogen atoms, and thereby exhibit preferential affinity to the negative Cr_2O_3 surface. In contrast, all acidic residues lose their protons at pH = 7, which results in negative charges, and thereby exhibit repulsion to the negative Cr_2O_3 surface.

Armed with the understanding that basic and acidic amino acid residues exhibit distinctly different adsorption behaviors onto Cr_2O_3, the corresponding interaction energies were calculated, as displayed in Fig. 7. Specifically, lysozyme contains three types of basic amino acid residues (namely, lysine, arginine, and histidine), and each data point in Fig. 7a represents the sum of interaction energies of all these residues in lysozyme. Analogously, Fig. 7b presents the summation of the interaction energies of all the acidic residues (namely, acetic acid and glutamic acid). Furthermore, Fig. S10 and S11 present the Coulombic and Lennard-Jones components that sum up the total interaction energies.

A key highlight of Fig. 7 is that the interaction energies of the basic amino acid residues are negative, whereas those of the acidic ones are positive. This implies that basic residues are attracted to Cr_2O_3, but acidic ones interact repulsively with Cr_2O_3. In agreement with Fig. 3b, Fig. S10 and S11 show that the Coulombic components (i.e., −25 to −270 kJ/mol for basic residues, and 0–44 kJ/mol for acidic residues) are significantly more dominant than the Lennard-Jones ones (i.e., 6 to −20 kJ/mol for basic residues, and 0 to −13 kJ/mol for acidic residues) for both residue types, implying similarly that charge interactions are more influential on the adsorption behavior. Three other observations are interesting. Firstly, regarding Orientations 1 and 4, their overall relatively less attractive interaction energies shown in Fig. 3a are tied to the relatively lower attraction (−25 to −45 kJ/mol) of the basic residues (Fig. 7a) and relatively higher repulsion (+10 to +35 kJ/mol) of the acidic residues (Fig. 7b). Secondly, the repulsive energies of the acidic amino acids are almost zero for Orientations 3 and 6, because the acidic

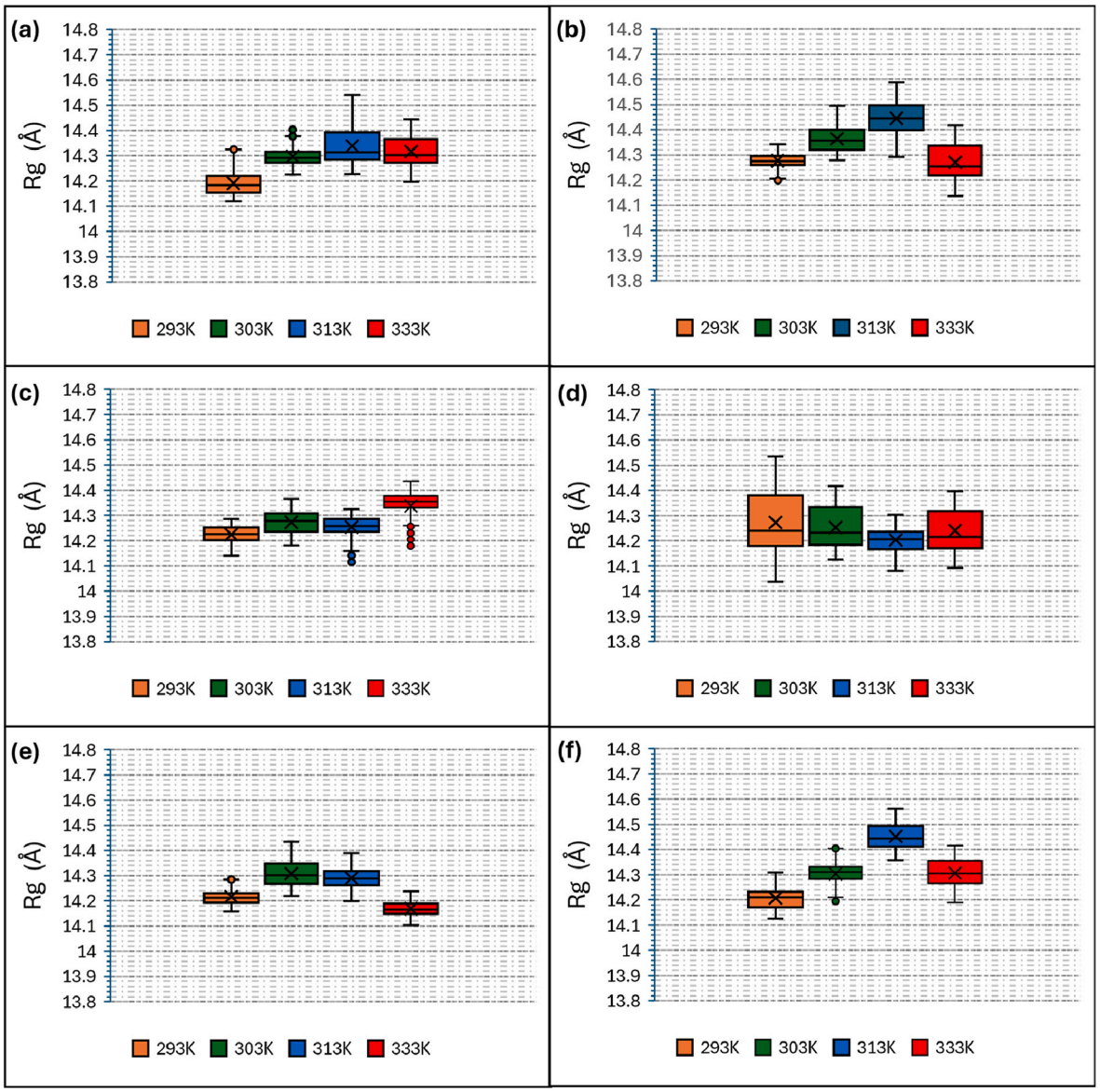

Fig. 9. Box plots of the radius of gyration (Rg) of lysozyme-Cr_2O_3 (10 ns - 100 ns) for six initial orientations at four different temperatures. **a-f** represent Orientations 1–6.

amino acids tend not to get close to Cr_2O_3 (Fig. 6b), and the lack of repulsion contributes to the lowest total interaction energies among all the cases exhibited at 303 K for these two orientations (Fig. 3a). Thirdly, the relatively lower impact of temperature on the total interaction energies for Orientations 1 and 2 (Fig. 3a) appears tied to the corresponding low impact of temperature on the interactions of the basic residues (Fig. 7a). In summary, Fig. 7 demonstrates the general dominance of the attraction of the basic amino acid residues to Cr_2O_3 in governing the adsorption by lysozyme.

3.6. Additional characterizations

Fig. 8 presents the evolution of root-mean-square deviation (rmsd), which reflects the mobility of lysozyme attributable to various phenomena, such as conformational changes, lysozyme-Cr_2O_3 interactions, etc. Also, the rmsd trends in the absence of Cr_2O_3 are shown in Fig. S12. In addition, Fig. S13 and S14 display the root-mean-square fluctuation (rmsf) of each amino acid residue in lysozyme in the presence and absence of the Cr_2O_3 slab, which reflects the flexibility of the lysozyme chain.

Without the Cr_2O_3, higher temperatures increase rmsd values, specifically in that the upper rmsd limits are approximately 1.3 Å at 293 K and 303 K, whereas greater at 1.6 Å for the higher temperatures of 313 K and 333 K. On average, the rmsd values fluctuate about 1.2 Å, reflecting the mobility of a free lysozyme in the solution. Furthermore, Fig. S13 and S14 show most of the residues are distinctly more mobile without the Cr_2O_3 slab. In particular, at the temperature of 333 K (Fig. S13d and S14d), the flexibility of the lysozyme chain is more significantly restricted by Cr_2O_3.

Compared to the absence of the Cr_2O_3 slab, the range of rmsd values broadened due to the attractive and repulsive interaction of lysozyme with the Cr_2O_3 slab (Fig. 8). The depressed lower rmsd limits of down to 0.8 Å reflect the adsorption of lysozyme onto the Cr_2O_3 slab, which restricts mobility. For instance, in the case of Orientation 3 at 313 K, the rmsd values are hardly above 1 Å, which is distinctly lower than that of lysozyme without the Cr_2O_3 slab (Fig. S12). This indicates relatively stable adsorption at this temperature, as also evident in the relatively depressed rmsf values in Fig. S14c, even though the interaction energy is not the most negative (Fig. 3a). As another instance, Orientation 1 at 293–303 K exhibits relatively low rmsd values, with the low mobility

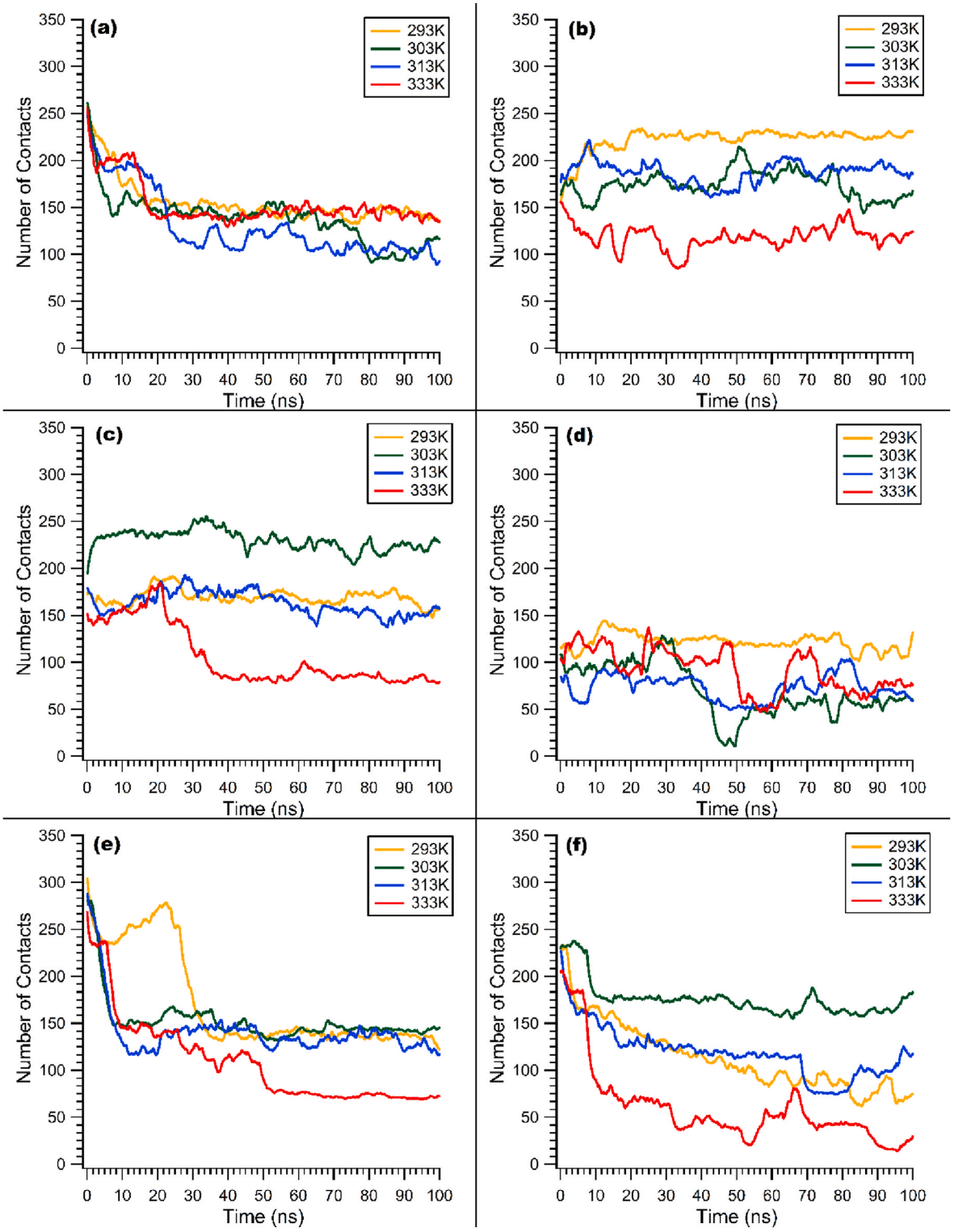

Fig. 10. Number of lysozyme-Cr_2O_3 contacts over time for six initial orientations at four different temperatures. **a-f** represent Orientations 1–6.

attributable to rmsf values of the residues being generally lower or equal to that in the absence of Cr_2O_3 (Fig. S13a–b). On the other hand, the elevated upper rmsd limits of up to 2 Å reflect repulsion from the Cr_2O_3 slab. For example, in the case of Orientation 2 at 313 K, although the interaction energy is rather attractive (Fig. 3a), the higher rmsd (Fig. 8b) and rmsf (Fig. S14c) values suggest lysozyme remains highly mobile. The higher mobility and flexibility may ease induced desorption during cleaning of the FFE.

Radius of gyration (Rg) can be determined to understand the size and conformation changes of lysozyme. While Fig. S1 suggests visually minimal structural changes of the lysozyme molecule over the 100 ns run, Rg serves to quantify the structural evolution. Fig. S16 presents the evolution of the Rg values of the lysozyme-Cr_2O_3 systems for six initial orientations at four different temperatures, while Fig. S15 presents that in the absence of Cr_2O_3. The similarity of the Rg values in the absence and presence of the Cr_2O_3 slab reflects the adsorption or lack thereof of

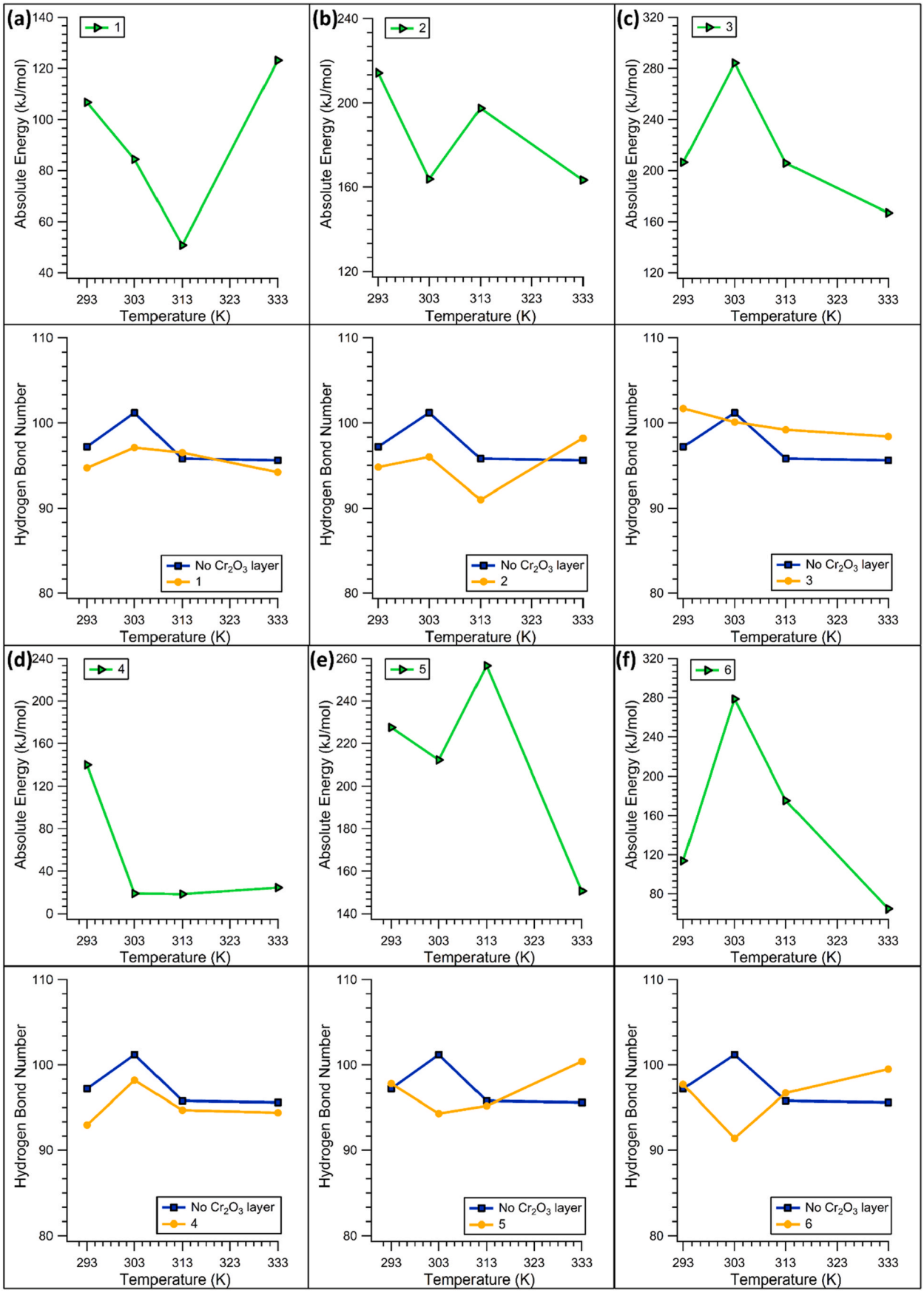

Fig. 11. Number of intra-lysozyme hydrogen bonds in the absence and presence of the Cr_2O_3 slab along with the absolute total interaction energies for all orientations at different temperatures.

lysozyme causes negligible conformational changes to the lysozyme molecule. Additionally, Fig. 9 presents the box plots corresponding to Fig. S16. The error bars reflect some perturbation of the lysozyme structure, but the extents are not significant. In the case without Cr_2O_3, similar to the mobility behavior demonstrated by rmsd analysis, limited flexibility of lysozyme is observed at 293 K and 303 K, whereas larger conformational changes are observed at the higher temperatures of 313 K and 333 K (Fig. S15). The interaction of lysozyme with Cr_2O_3 generally causes a slight increase in Rg values from approximately 14.2 to 14.4 Å, increasing the upper Rg limit to 14.6 Å. This suggests a change in the shape of lysozyme due to adsorption onto Cr_2O_3. Even at the highest temperature of 333 K, Rg values remain similar, indicating conformational stability.

The number of lysozyme-Cr_2O_3 contacts (defined as when the minimum distance is less than 6 Å), which reflect the number of interacting atoms between the two entities, is presented in Fig. 10. Overall, the number of contacts ranges between approximately 15 and 240. While temperature has the least effect on Orientation 1 (Fig. 10a), the effect is significant on Orientation 3 (Fig. 10c). The least negative interaction energies (Fig. 3a) corresponding to Orientation 4 at 303–333 K give relatively low contacts of 55, 65, and 80 respectively at 303 K, 313 K, and 333 K. However, the lowest number of contacts is 15 for the case of Orientation 6 at 333 K, which corresponds to a relatively more attractive interaction energy. The seeming contradiction can be traced to a higher number of basic contacts (Fig. 6) with attractive energies. Nonetheless, when the interaction energies (Fig. 3a) and contact numbers (Fig. 10) are compared internally and orientation-specific, it is evident that interaction energy magnitude and contact number are positively correlated.

Intra-lysozyme hydrogen bond is important for secondary and tertiary conformational stability. Changes in the number of internal hydrogen bonds provides information about the folding state and interaction with the environment. The number of intra-lysozyme hydrogen bonds in the presence and absence of Cr_2O_3 is presented in Fig. 11. At 303 K, the number of hydrogen bonds in the absence of Cr_2O_3 is highest for all orientations, which indicates the most tightly bound, stable lysozyme. Generally, the number of hydrogen bonds in the absence of the Cr_2O_3 slab is higher than that in the presence, which is tied to lysozyme adsorption onto Cr_2O_3 and thus reflects some slight structural adjustments of the lysozyme molecule upon adsorption. Specifically, amino acid residues like lysine, arginine, and serine which are instrumental in the intra-lysozyme hydrogen bonds, become involved in interacting with Cr_2O_3 and thus diminishing the hydrogen bonds in the free lysozyme. Correspondingly, higher-Cr_2O_3 lysozyme interaction energies (Fig. 3a) are correlated with lower number of hydrogen bonds.

4. Conclusion

This MD simulation study investigated the adsorption behavior of lysozyme on a Cr_2O_3 surface at four different temperatures and six initial orientations.

Key observations indicate that local interactions, driven predominantly by Coulombic forces, are crucial in governing adsorption. Basic amino acids, particularly lysine and arginine, were found to play a dominant role due to their strong electrostatic attraction to the negatively charged Cr_2O_3 surface. Conversely, acidic amino acids demonstrated weaker repulsive interactions due to the inherent negative charge at neutral pH.

Temperature effects were shown to be secondary to local interactions, with no clear correlation with adsorption behaviors. While higher temperatures generally reduced adsorption for some orientations, the specific spatial arrangements and local amino acid residues play more crucial roles in governing adsorption. It should be noted that the lack of temperature influence on adsorption suggests the onset of fouling is temperature-independent, but the underlying mechanisms of whether and how subsequent fouling stages of aggregation and layering are affected by temperature require further investigation.

The adsorption process was further confirmed through minimum distance and binding energy analyses, highlighting that strong interactions are characterized by shorter distances between the protein and surface. Additionally, the root-mean-square deviation (rmsd) and radius of gyration (Rg) analyses indicate that adsorption had minimal impact on the lysozyme's secondary structure, further emphasizing the role of side-chain interactions in stabilizing adsorption.

Overall, this study underscores the significance of local electrostatic interactions, particularly involving basic residues, in dictating the adsorption behavior of lysozyme onto the Cr_2O_3 surface. The findings provide insights into the local adsorption tendencies of lysozyme, and thereby the incipient fouling behaviors, which are expected to be valuable towards addressing the inevitable fouling challenge in the FFE-processing of emerging food protein formulations. For more in-depth understanding of macroscopic phenomena like heat transfer and foulant buildup in future, MD simulations can be bridged with continuum models.

CRediT authorship contribution statement

Mütesir Temel: Writing – original draft, Visualization, Validation, Resources, Methodology, Investigation, Formal analysis, Data curation. **Sadiye Velioğlu:** Writing – review & editing, Validation, Resources. **Anders Hellman:** Writing – review & editing, Supervision. **Jia Wei Chew:** Writing – review & editing, Validation, Supervision, Project administration, Methodology, Investigation, Funding acquisition, Formal analysis, Conceptualization.

Declaration of competing interest

The authors declare that they have no known competing financial interests or personal relationships that could have appeared to influence the work reported in this paper.

Acknowledgements

We are grateful for funding from the Swedish Research Council (2024–04273), and Chalmers Gender Initiative for Excellence (Genie). The numerical calculations reported in this paper were performed using TUBITAK ULAKBIM (High Performance and Grid Computing Center TRUBA resources). We also acknowledge Andres Dahlin and John Andersson from Chalmers University of Technology for valuable discussions on QCM-D.

Appendix A. Supplementary data

Supplementary data to this article can be found online at https://doi.org/10.1016/j.jfoodeng.2025.112816.

Data availability

Data will be made available on request.

References

A. L. and S. P. and J. R., Crowley, O.J.A., Kelly, S.V., 2016. Rehydration and solubility characteristics of high-protein dairy powders. In: McSweeney, J.A., Paul, L.H., Mahony, O. (Eds.), Advanced Dairy Chemistry: Volume 1B: Proteins: Applied Aspects. Springer New York, New York, NY, pp. 99–131. https://doi.org/10.1007/978-1-4939-2800-2_4.

Antosiewicz, J.M., Długosz, M., 2020. Constant-pH brownian dynamics simulations of a protein near a charged surface. ACS Omega 5 (46), 30282–30298. https://doi.org/10.1021/acsomega.0c04817.

Best, R.B., et al., 2012. Optimization of the additive CHARMM all-atom protein force field targeting improved sampling of the backbone φ, ψ and side-chain χ1 and χ2 dihedral angles. J Chem Theory Comput 8 (9), 3257–3273. https://doi.org/10.1021/ct300400x.

Brooks, B.R., Bruccoleri, R.E., Olafson, B.D., States, D.J., Swaminathan, S., Karplus, M., 1983. CHARMM: a program for macromolecular energy, minimization, and dynamics calculations. J. Comput. Chem. 4 (2), 187–217. https://doi.org/10.1002/jcc.540040211.

Cassano, A., Rastogi, N.K., Basile, A., 2020. Reverse osmosis in food processing. Current Trends and Future Developments on (Bio-) Membranes: Reverse and Forward Osmosis: Principles, Applications, Advances 229–257. https://doi.org/10.1016/B978-0-12-816777-9.00010-1.

Chew, J.W., Kilduff, J., Belfort, G., 2020. The behavior of suspensions and macromolecular solutions in crossflow microfiltration: an update. J Memb Sci 601, 117865. https://doi.org/10.1016/J.MEMSCI.2020.117865.

Cummings, P.T., et al., 2021. Open-source molecular modeling software in chemical engineering focusing on the molecular simulation design framework. AIChE J. 67 (3), e17206. https://doi.org/10.1002/aic.17206.

Cyklis, P., 2022. Effect of fouling on falling film evaporator performance in industrial conditions of fruit juice concentrate production. J. Food Eng. 317, 110884. https://doi.org/10.1016/J.JFOODENG.2021.110884.

Dantas, A., Costa, D.P., Felipe, X., Gou, P., 2024. Innovations in spray drying technology for liquid food processing: design, mechanisms, and potential for application. Applied Food Research 4 (1), 100382. https://doi.org/10.1016/J.AFRES.2023.100382.

Darden, T., York, D., Pedersen, L., 1993. Particle mesh ewald: an n·log(N) method for ewald sums in large systems. J. Chem. Phys. 98 (12), 10089–10092. https://doi.org/10.1063/1.464397.

De Jong, P., 1997. Impact and control of fouling in milk processing. Trends Food Sci. Technol. 8 (12), 401–405. https://doi.org/10.1016/S0924-2244(97)01089-3.

Díaz-Ovalle, C.O., González-Alatorre, G., Alvarado, J.F.J., 2017. Analysis of the dynamic response of falling-film evaporators considering fouling. Food Bioprod. Process. 104, 124–136. https://doi.org/10.1016/j.fbp.2017.05.007.

Eleftheriou, M., Germain, R.S., Royyuru, A.K., Zhou, R., 2006. Thermal denaturing of mutant lysozyme with both the OPLSAA and the CHARMM force fields. J. Am. Chem. Soc. 128 (41), 13388–13395. https://doi.org/10.1021/ja060972s.

Fasolin, L.H., et al., 2019. Emergent food proteins – towards sustainability, health and innovation. Food Res. Int. 125, 108586. https://doi.org/10.1016/j.foodres.2019.108586.

Gulied, M., et al., 2023. A review of membrane-based dewatering technology for the concentration of liquid foods. J. Environ. Chem. Eng. 11 (5), 110583. https://doi.org/10.1016/J.JECE.2023.110583.

Jebson, R.S., Iyer, M., 1991. Performances of falling film evaporators. J. Dairy Res. 58 (1), 29–38. https://doi.org/10.1017/S0022029900033483.

Kanhaiya, K., Kim, S., Im, W., Heinz, H., 2021. Accurate simulation of surfaces and interfaces of ten FCC metals and steel using lennard–jones potentials. npj Comput. Mater. 7 (1). https://doi.org/10.1038/s41524-020-00478-1.

Ledenbach, L.H., Marshall, R.T., 2009. Compendium of the microbiological spoilage of foods and beverages. Compendium of the Microbiological Spoilage of Foods and Beverages. https://doi.org/10.1007/978-1-4419-0826-1.

Lewis, M., 2023. Chapter 3 - foods and food processing. In: Lewis, D. (Ed.), M. B. T.-F. P. E. P. 13–19. https://doi.org/10.1016/B978-0-12-821182-3.00028-5. Woodhead Publishing.

Liu, W., Delaplace, G., 2024a. Fouling in the dairy industry. Milk and Dairy Products 193–259. https://doi.org/10.1002/9781394312405.CH6.

Liu, W., Delaplace, G., 2024b. Fouling in the dairy industry. In: Milk and Dairy Products. John Wiley & Sons, Ltd, pp. 193–259. https://doi.org/10.1002/9781394312405.ch6 ch. 6.

Loveday, S.M., 2019. Food proteins: technological, nutritional, and sustainability attributes of traditional and emerging proteins. Annu. Rev. Food Sci. Technol. 10, 311–339. https://doi.org/10.1146/annurev-food-032818-121128.

Ma, Y., Chew, J.W., 2022a. Investigation of membrane fouling phenomenon using molecular dynamics simulations: a review. J Memb Sci 661, 120874. https://doi.org/10.1016/j.memsci.2022.120874.

Ma, Y., Chew, J.W., 2022b. Investigation of membrane fouling phenomenon using molecular dynamics simulations: a review. J Memb Sci 661, 120874. https://doi.org/10.1016/J.MEMSCI.2022.120874.

Ma, Y., Zydney, A.L., Chew, J.W., 2021a. Membrane fouling by lysozyme: effect of local interaction. AIChE J. 67 (7), e17212. https://doi.org/10.1002/aic.17212.

Ma, Y., Zydney, A.L., Wang, R., Chew, J.W., 2021b. Molecular dynamics study on membrane fouling by oppositely charged proteins. AIChE J. 67 (10), e17335. https://doi.org/10.1002/aic.17335.

Miyawaki, O., Inakuma, T., 2021. Development of progressive freeze concentration and its application: a review. Food Bioproc Tech 14 (1), 39–51. https://doi.org/10.1007/S11947-020-02517-7/TABLES/9.

Morison, K.R., 2015a. Reduction of fouling in falling-film evaporators by design. Food Bioprod. Process. 93, 211–216. https://doi.org/10.1016/J.FBP.2014.10.009.

Morison, K.R., 2015b. Reduction of fouling in falling-film evaporators by design. Food Bioprod. Process. 93, 211–216. https://doi.org/10.1016/j.fbp.2014.10.009.

Panczyk, T., Nieszporek, J., Nieszporek, K., 2022. Molecular dynamics simulations of interactions between human telomeric i-Motif deoxyribonucleic acid and functionalized graphene. J. Phys. Chem. B 126 (35), 6671–6681. https://doi.org/10.1021/acs.jpcb.2c04327.

Qiu, H., et al., 2022. Functional polymer materials for modern marine biofouling control. Prog. Polym. Sci. 127, 101516. https://doi.org/10.1016/J.PROGPOLYMSCI.2022.101516.

Rabe, M., Verdes, D., Seeger, S., 2011. Understanding protein adsorption phenomena at solid surfaces. Adv. Colloid Interface Sci. 162 (1–2), 87–106. https://doi.org/10.1016/J.CIS.2010.12.007.

Sahihi, M., Faraudo, J., 2022. Computer simulation of the interaction between SARS-CoV-2 spike protein and the surface of coinage metals. Langmuir 38 (48), 14673–14685. https://doi.org/10.1021/acs.langmuir.2c02120.

Sim, J.W., Lee, H., Jo, S., Oh, S., Kim, S., Kim, D.R., 2023. Increasing energy saving of pilot-scale spray dryers with enhanced yield by low-adhesive surfaces. Case Stud. Therm. Eng. 49, 103218. https://doi.org/10.1016/J.CSITE.2023.103218.

Singh, A., Vanga, S.K., Orsat, V., Raghavan, V., 2018. Application of molecular dynamic simulation to study food proteins: a review. Crit. Rev. Food Sci. Nutr. 58 (16), 2779–2789. https://doi.org/10.1080/10408398.2017.1341864.

Toukan, K., Rahman, A., 1985. Molecular-dynamics study of atomic motions in water. Phys. Rev. B 31 (5), 2643–2648. https://doi.org/10.1103/PhysRevB.31.2643.

Tuoc, T.K., 2015. Fouling in dairy processes. Mineral Scales and Deposits: Scientific and Technological Approaches, pp. 533–556. https://doi.org/10.1016/B978-0-444-63228-9.00020-6.

Utesch, T., Millo, D., Castro, M.A., Hildebrandt, P., Zebger, I., Mroginski, M.A., 2013. Effect of the protonation degree of a self-assembled monolayer on the immobilization dynamics of a [NiFe] hydrogenase. Langmuir 29 (2), 673–682. https://doi.org/10.1021/la303635q.

Wei, T., Carignano, M.A., Szleifer, I., 2012. Molecular dynamics simulation of lysozyme adsorption/desorption on hydrophobic surfaces. J. Phys. Chem. B 116 (34), 10189–10194. https://doi.org/10.1021/jp304057e.

Wilson, D.I., 2018. Fouling during food processing – progress in tackling this inconvenient truth. Curr. Opin. Food Sci. 23, 105–112. https://doi.org/10.1016/J.COFS.2018.10.002.

Yildirim, N., Genc, S., 2017. Energy and exergy analysis of a milk powder production system. Energy Convers. Manag. 149, 698–705. https://doi.org/10.1016/J.ENCONMAN.2017.01.064.

Zhang, Z.Q., et al., 2022a. Protein conformation and electric attraction adsorption mechanisms on anodized magnesium alloy by molecular dynamics simulations. J. Magnesium Alloys 10 (11), 3143–3155. https://doi.org/10.1016/j.jma.2021.04.005.

Zhang, Y.-S., Chu, B.-S., Yu, H.-L., Li, K., Wang, W.-H., Yang, W., 2022b. Molecular dynamics simulations of the initial oxidation process on ferritic Fe–Cr alloy surfaces. RSC Adv. 12 (16), 9501–9511. https://doi.org/10.1039/D1RA09329K.

Zhou, H.-X., Pang, X., 2018. Electrostatic interactions in protein structure, folding, binding, and condensation. Chem Rev 118 (4), 1691–1741. https://doi.org/10.1021/acs.chemrev.7b00305.

Zhuang, W., et al., 2020. Interfacial microenvironment for lipase immobilization: regulating the heterogeneity of graphene oxide. Chem. Eng. J. 394, 125038. https://doi.org/10.1016/j.cej.2020.125038.